Segmentation of brain tumor images using in vivo spectroscopy, relaxometry and diffusometry by magnetic resonance

M. Martín-Landrove

Instituto de Resonancia Magnética, La Florida/San Román, Departamento de Espectroscopía y Desarrollo de Aplicaciones and Universidad Central de Venezuela,

Facultad de Ciencias, Escuela de Física, Centro de Resonancia Magnética, Grupo de Física Molecular, Apartado Postal 47586, Caracas 1041-A, Venezuela

Recibido el 10 de diciembre de 2003; aceptado el 19 de junio de 2004

A new methodology is developed for the segmentation of brain tumor images using information obtained by different magnetic resonance techniques such as in vivo spectroscopy, relaxometry and diffusometry. In vivo spectroscopy is used as a sort of virtual biopsy to characterize the different tissue types present in the lesion (active tumor, necrotic tissue or edema and normal or non-affected tissue). Due to the fact that in vivo spectroscopy information lacks the spatial resolution for treatment considerations, this information has to be combined or fused with images obtained by relaxometry and diffusometry with excellent spatial resolution. Some segmentation schemes are presented and discussed, using the high spatial resolution techniques individually or combined. The results show that segmentation done in this way is highly reliable for the application of future therapies such as radiosurgery or radiotherapy.

Keywords: Relaxometry; diffusometry; segmentation; magnetic resonance.

Se desarrolló una nueva metodología para la segmentación de imágenes de tumores en cerebro utilizando diferentes técnicas de imágenes por resonancia magnética, como son la espectroscopía in vivo, la relaxometría y la difusometría. La espectroscopía in vivo se utiliza como una especie de "biopsia virtual" para caracterizar cada uno de los tejidos presentes en la lesión (tumor activo, necrosis o edema y tejido no afectado). Esta información, sin embargo, carece de la resolución espacial suficiente para efectos de la terapia y por lo tanto debe ser combinada o fusionada con imágenes obtenidas por relaxometría y difusometría que presentan excelente resolución espacial. Diversos enfoques de segmentación son presentados y discutidos, utilizando las técnicas de alta resolución espacial por separado o en conjunto. Los resultados demuestran que este tipo de segmentación es de alta confiabilidad para la aplicación de futuras terapias como radiocirugía o radioterapia.

Descriptores: Relaxometría; difusometría; segmentación; resonancia magnética.

PACS: 87.61.-c; 82.56.Na; 82.56.Lz

1. Introduction

Magnetic Resonance Spectroscopy (MRS) is a method that assesses metabolic tissue information by analyzing the composition and spatial distribution of cellular metabolites [1]. MRS is a non-invasive tool that makes it possible to distinguish malignant brain tumors from non-anaplastic tumors. In recent years there have been numerous publications showing that MRS can detect significant differences between in vivo spectra of tumor, necrosis and normal brain tissue [2-9]. Metabolic maps can be obtained by the Chemical Shift Imaging (CSI) technique, which obtains, in one image, several spectra from a series of small voxels (matrix) from a large region of interest, but they lack the spatial resolution necessary for therapy purposes. Relaxation studies have been long used for the assessment of tumors, with the T_2-map of a tissue often used as a basis for interpreting clinical images [10]. Multiexponential T_2 decay occurs in NMR studies in both material [11-13] and biological systems [14,15]. Diffusion-weighted MRI has been used successfully in the central nervous system (CNS), especially in the diagnosis of acute stroke, but also in distinguishing different components of brain tumors [16-18]. In the present work, it is proposed the use of MRS, Relaxometry, and Diffusometry is proposed for the segmentation of brain tumors.

2. Image measurement

CSI was performed axially to obtain spatial distributions of metabolite concentration across the lesion, with TE = 30 ms and VOI of 96 cm^3 (80 $\times$ 80 $\times$ 15 mm). Relaxometry studies were performed using the standard multiecho sequence (CPMG) with 16 echoes, and a base echo time TE = 22 ms and 8 axial planes 5 mm thick centered at the tumor. The pixel intensity is given by

$$I = I_0 \exp\Big(- \frac{nTE}{T_2}\Big), \tag{1}$$

where n is the number of the echo and T_2 is the transversal relaxation time. Diffusion-weighted images were obtained for 16 b-parameter values ranging from 0 to 1350 s/mm^2 and 3 orthogonal magnetic field gradient directions (Phase, Read and Slice) for the same set of planes used in the relaxometry studies. In this case, the pixel intensity is given by

$$I = I_0 \exp\Big(- b_i D_{ii}\Big) \tag{2}$$

where i = p, r, s depending of the direction of the gradient, D_{ii} represents the corresponding diagonal component of the diffusion tensor, and b_i is

$$b_i = \gamma^2 G_i^2 \delta^2 \Big(\Delta - \delta/3\Big), \tag{3}$$

where γ is the gyromagnetic ratio, G_i is the magnitude of each of the gradient pulses that codify diffusion, δ is the gradient pulse width and Δ is the time interval between gradient pulses. The spectroscopy data analysis was performed based on relative values. The critical Cho/NAA ratio value for which a tissue was considered malignant was 1.3 or over. The spectra were considered atypical if the Cho/NAA ratio had a value between 0.9 and 1.29. For the analysis of relaxation and diffusion data, a special image processing algorithm was developed to extract the magnetization decays for different regions of interest or ROI´s. They were processed by an Inverse Laplace Transform (ILT) algorithm [19-21] to obtain the relaxation rates or diffusion tensor components present in the lesion. For each voxel the set of parameters obtained were assigned to a different state of the tissue (normal, pathologic, necrotic or edema) on comparison with the CSI data, using it as a sort of virtual biopsy.

3. Segmentation procedure

In order to perform the segmentation, the different types of tissues have to be identified on the image. A RGB color code is selected to indicate the existence of pathology: R (red) corresponds to tumor, G (green) to normal or unaffected tissue, and B (blue) corresponds to edema or necrosis [22]. The selection of the color code is completely arbitrary and somewhat troublesome for clinical purposes, as will be disscused below. Instead of applying the ILT algorithm pixel by pixel, which is a time consuming procedure with a low signal to noise ratio, the following assumption was made: let us suppose that the image intensity in each pixel (in a set of multiecho or multi-b images) is a linear superposition of the different decaying exponential functions, each one characterized by a decay parameter (relaxation rate or diffusion tensor component) corresponding to the different tissues

$$I(t) = bl + A_R X_R(t) + A_G X_G(t) + A_B X_B(t) \qquad (4)$$

where

$$X_i(t) = \exp(-\lambda_i t) \qquad (5)$$

with i = R, G or B, λ_i is the decay parameter associated with the different tissues and extracted from the average decay parameter spectrum, bl is a parameter introduced to take into account corrections in the baseline of the image intensity (also done in the application of the ILT algorithm) and the coefficients A_i, which are positive, determine the proportion of each decay in the image. By a linear regression procedure, the coefficients A_i are determined for each pixel in the image. Particular attention was paid to the correlation coefficient in the linear regression analysis, and in the present work, the coefficients A_i were only accepted for those fittings with a squared correlation coefficient of over 0.99. To further assess the segmentation procedure and in order to eliminate spurious "tumor positive" pixels due to the fact that the exponential functions are correlated, each pixel affected by the presence of the tumor, *i.e.*, its coefficient A_R is different from zero, is averaged over its neighborhood and accepted as a true "tumor positive" if and only if its average p is greater than 1/3. This kind of filter allows for a more compact segmentation of the tumor and discards scattered "tumor positive" points in the image.

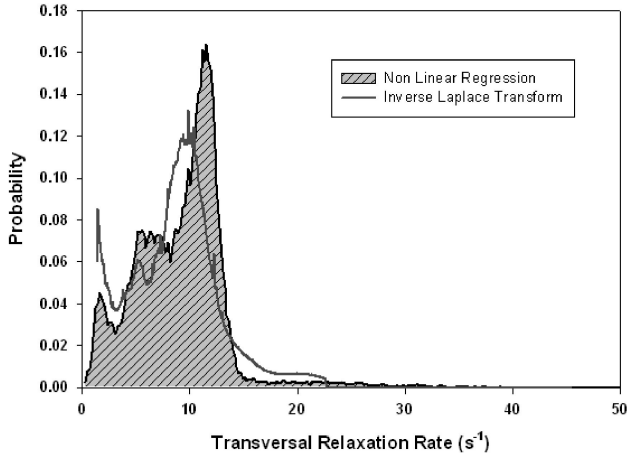

FIGURE 1. Comparison of relaxation spectrum obtained by the ILT algorithm and non linear regression analysis.

4. Results and discussion

For a total of 10 patients, the relaxation rates were within the following ranges: for edema or necrotic tissue, 0.65 - 3.43 s^{-1}, for tumor tissue, 5.05 - 7.47 s^{-1}, and for normal or non affected tissue (gray/white matter or meningeal tissue), 8.67 - 25.26 s^{-1}. Typical values for the average p covered a range 0.71 - 0.96. Control values of p were found in the range of 0.44 - 0.69. To validate the ILT algorithm, non linear regression analyses were performed over relaxation data assuming a single exponential decay, a common situation found in commercial postprocessing software. A typical result is depicted in Fig. 1. Although the relaxation spectra are qualitatively similar, the actual values for the relaxation rates differ noticeably, and the ILT algorithm is preferred for the segmentation procedure. Fig. 2 shows a result of the segmentation procedure.

Instead of using a color map in Fig. 2, as explained in the preceding section, the RGB code is mapped on a gray scale as follows: as a first step is determined the maximum among the A_i coefficients; depending on the result its value is mapped in the following ranges: A_R in 206 - 255 (light gray), A_G in 51 - 205 (gray), and A_B in 0 - 50 (dark gray). The reason for following, this kind of procedure is based on the fact that radiologists are mainly trained to analyze gray scale images and some of the information present in the color RGB code has to be expended in favor of a better understanding of the image by the physician. In particular,the mapping chosen in this work resembles gadolinium contrasted images, which are commonly used in tumor detection by MRI. In addition, it preserves all the anatomical details of the image (as in the

color coded), which are of relevance for image registration or fusion procedures, commonly used in therapy planning. A different kind of segmentation is shown in Fig. 3, where only the "tumor positive" pixels are depicted or contour intensity plots for the intensity of the parameter A_R.

The segmentation based on diffusion-weighted images is a little more troublesome, mainly due to the fact that diffusion is in general anysotropic in tissue and the segmentation depends on the actual gradient direction, as shown in Fig. 4. In order to deal with scalar quantities (as is done for relaxation), the diffusion- weighted images corresponding to the three orthogonal directions (P,R,S) are combined into a single set of diffusion-weighted images corresponding to the trace of the diffusion tensor, or more precisely to the average value of the diagonal terms given by

$$< D_{ii} >= Tr(D)/3 \tag{6}$$

and it is now posible to use exactly the same segmentation procedure as for relaxation. The comparison of the segmentation for relaxometry and diffusometry on the same slice are shown in Fig. 5.

It is evident that the segmentation is dependent on the selection of relaxation or diffusion-weighted data. Tumoral and necrotic tissue can exhibit very similar apparent diffusion coefficients, due to the fact that in general these tissues are less structured or organized than normal or unaffected tissues. The distribution of apparent diffusion coefficients over the lesion is shown in Fig. 6.

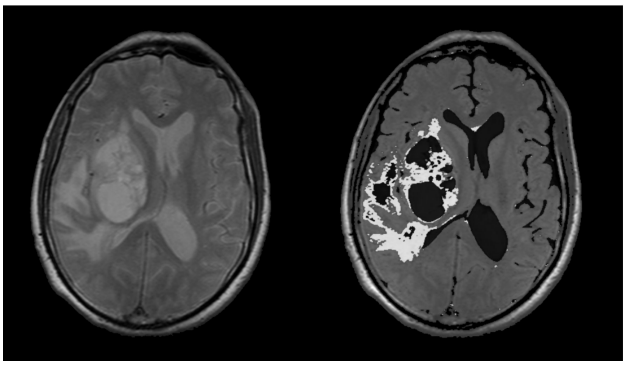

FIGURE 2. Left, multiecho image for TE=44 ms. Right, segmented image.

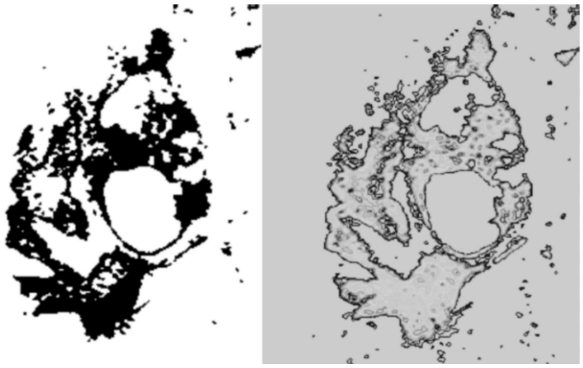

FIGURE 3. Left, segmentation showing "tumor positive" pixels only. Right, contour plots.

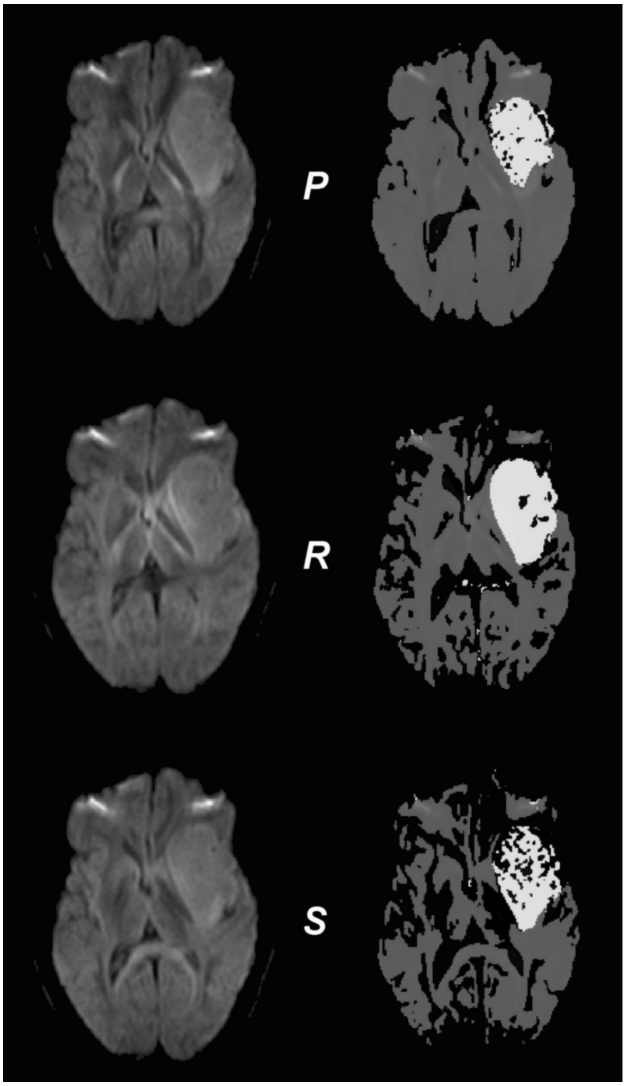

FIGURE 4. Diffusion-weighted images, left and segmented images, right for gradients P,R,S.

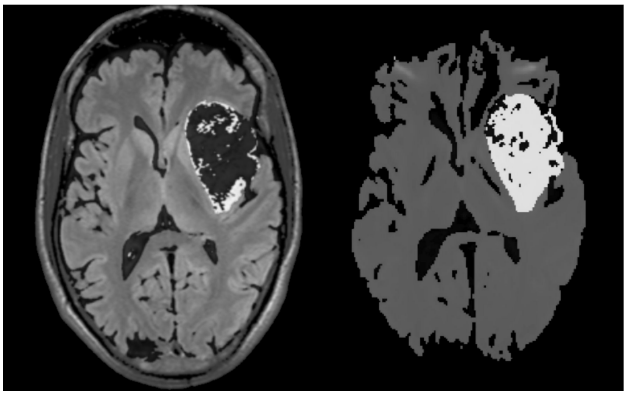

FIGURE 5. Left, segmented image using relaxation data. Right, segmented image using the trace of the diffusion tensor.

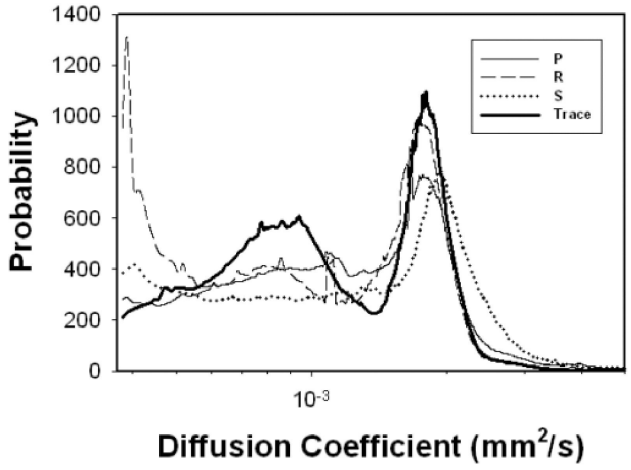

FIGURE 6. Distributions of diffusion coefficient.

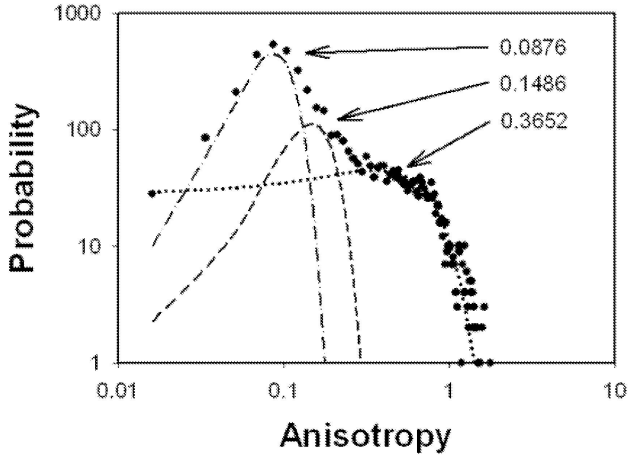

FIGURE 7. Distribution of α.

The same happens if other scalar quantities are considered, such as fractional anisotropy or relative anisotropy [23,24], that require the full determination of the diffusion tensor and so are beyond the scope of this work, *i.e.*, only the diagonal terms of the diffusion tensor are determined. Nevertheless, diffusion-weighted images can be used to define clearly what corresponds to unaffected tissue which exhibits high anisotropy as opposed to tumoral or necrotic tissue with low anisotropy. A possible definition of anisotropy, not necessarily a scalar quantity, can be written as

$$\alpha = \Big(\frac{\Delta_{xy}^2 + \Delta_{yz}^2 + \Delta_{xz}^2}{(Tr(D))^2/3}\Big)^{1/2} \tag{7}$$

where $\Delta_{ij} = D_{ii} - D_{jj}$. Figure 7 shows the resultant distribution of anisotropy.

It is suggested that a consensus be taken between relaxation and diffusion-weighted data to define the segmentation of the tumor in the image.

5. Conclusions

The methodology presented in this work clearly segments brain tumor images with appropriate spatial resolution for therapeutical needs. Other parameters, such as anisotropy can be considered to further improve the segmentation quality, but depends on the software available to the MRI facility. Finally, image registration for different data such as relaxometry or diffusometry seems to be the best way to assess a reliable segmentation of the tumor image.

Acknowledgments

The author would like to thank the technicians Valentina Itriago and Rolando Cedeño for their further collaboration and helpful skills in acquiring the images.

1. B.D. Ross and T. Michaelis, *Magn. Reson. Q.* **10** (1994) 191.
2. J.F. Norfray *et al.*, *AJR Am. J. Roentgenol.* **173** (1999) 119.
3. M. Castillo, L. Kwock, and S.K. Mukherji, *AJNR Am. J. Neuroradiol.* **17** (1996) 1.
4. M. Castillo *et al.*, *Magn. Reson Imaging Clin. North Am.* **6** (1998) 1.
5. P.B. Barker, J.D. Glickson, and R.N. Bryan, *Magn. Reson. Imaging* **5** (1993) 32.
6. M. Castillo and L. Kwock, *Neuroimag. Clin. North Am.* **4** (1998) 733.
7. D.G. Kim *et al.*, *Neurosurgery* **46** (2000) 329.
8. G. Hagberg, *NMR in Biomedicine* **11** (1998) 148.
9. A.R. Tate *et al.*, *NMR in Biomedicine* **11** (1998) 117.
10. Z.-H. Chee, J.P. Jones, and M. Singh, *Foundations of Medical Imaging* (New York: Wiley, 1993).
11. T. Watanabe, N. Murase, M. Staemmler, and K. Gersonde, *Magn. Reson. Med.* **27** (1992) 118.
12. Kuhn W., Barth P., Denner P., Muller R., Sol. St. NMR **6** (1996) 295.
13. A.M. Luciani *et al.*, *Phys. Med. Biol.* **41** (1996) 509.
14. K.H. Cheng, *Magn. Reson. Med.* **12** (1994) 1099.
15. M.D. Does and J. Sayder, *Magn. Reson. Med.* **35** (1996) 207.
16. R.D. Tien, G.J. Felsberg, H. Friedman, M. Brown, and J. MacFall, *AJR Am. J. Roentgenol.* **162** (1994) 671.
17. J.S. Tsuruda, W.M. Chew, M.E. Moseley, and D. Norman, *AJR Am. J. Roentgenol.* **155** (1990) 1059.
18. S.E. Maier *et al.*, *Radiology* **219** (2001) 842.
19. M. Martín-Landrove, R. Martín, and A. Benavides, Proceedings of the International Society of Magnetic Resonance XIIth Meeting Part I, *Bull. Magn. Reson.* **17** (1995) 73.

20. I. Bonalde, M. Martín-Landrove, A. Benavides, R. Martín, and J. Espidel, *J. Appl. Phys.* **78** (1995) 6033.

21. R. Martín and M. Martín-Landrove, *Spatially Resolved Magnetic Resonance* (Wiley-VCH, New York,1998) Chap. 11, p. 133.

22. M. Martín-Landrove, I. Bautista, F. Mayobre, R. Villalta, and A. Contreras, *Magnetic Resonance Materials in Physics, Biology and Medicine* **15** (2002) 23.

23. P.J. Basser and C. Pierpaoli, *J. Magn. Reson. B* **111** (1996) 209.

24. T.E. Conturo, R.C. McKinstry, E. Akbudak, and B.H. Robinson, *Mag. Reson. Med.* **35** (1996) 399.